NIH RELAIS Document Delivery

NIH-10071780

NIH -- W1 SC653

PAMELA GEHRON ROBEY
CSDB/NIDR/NIH Bldng 30 Rm 228
30 CONVENT DRIVE MSC 4320
BETHESDA, MD 20892

ATTN:
PHONE: 301-496-4563
FAX: 301-402-0824
E-MAIL:

SUBMITTED: 2001-11-19 16:19:49
PRINTED: 2001-11-20 12:55:43
REQUEST NO.: NIH-10071780
SENT VIA: LOAN DOC
5052818

NIH Fiche to Paper Journal

TITLE:	SCIENCE
PUBLISHER/PLACE:	American Association For The Advancement Washington Dc
VOLUME/ISSUE/PAGES:	1994 Sep 2;265(5177):1405-12 1405-12
DATE:	1994
AUTHOR OF ARTICLE:	Coleman DE; Berghuis AM; Lee E; Linder ME; Gilman AG; Sprang
TITLE OF ARTICLE:	Structures of active conformations of Gi alpha 1 a
ISSN:	0036-8075
OTHER NOS/LETTERS:	Library reports holding volume or year 0404511 8073283
SOURCE:	PubMed
CALL NUMBER:	W1 SC653
REQUESTER INFO:	AB424
DELIVERY:	E-mail: probey@DIR.NIDCR.NIH.GOV
REPLY:	Mail:

Structures of Active Conformations of $G_{i\alpha 1}$ and the Mechanism of GTP Hydrolysis

David E. Coleman, Albert M. Berghuis, Ethan Lee, Maurine E. Linder,* Alfred G. Gilman, Stephen R. Sprang†

Mechanisms of guanosine triphosphate (GTP) hydrolysis by members of the G protein α subunit–$p21^{ras}$ superfamily of guanosine triphosphatases have been studied extensively but have not been well understood. High-resolution x-ray structures of the GTPγS and GDP·AlF_4^- complexes formed by the G protein $G_{i\alpha 1}$ demonstrate specific roles in transition-state stabilization for two highly conserved residues. Glutamine^{204} (Gln^{61} in $p21^{ras}$) stabilizes and orients the hydrolytic water in the trigonal-bipyramidal transition state. Arginine 178 stabilizes the negative charge at the equatorial oxygen atoms of the pentacoordinate phosphate intermediate. Conserved only in the G_α family, this residue may account for the higher hydrolytic rate of G_α proteins relative to those of the $p21^{ras}$ family members. The fold of $G_{i\alpha 1}$ differs from that of the homologous $G_{t\alpha}$ subunit in the conformation of a helix-loop sequence located in the α-helical domain that is characteristic of these proteins; this site may participate in effector binding. The amino-terminal 33 residues are disordered in GTPγS-$G_{i\alpha 1}$, suggesting a mechanism that may promote release of the βγ subunit complex when the α subunit is activated by GTP.

G proteins, which act as transducers and timers in transmembrane signaling systems, adopt a remarkable signaling strategy in which a metastable GTP-bound conformational state of the α subunit is exploited as an information carrier (*1–3*). Signaling is terminated when GTP is hydrolyzed to guanosine diphosphate (GDP) by the G protein α subunit, and it is thus crucial to stall catalysis at the threshold of the transition state to produce a molecular species that specifically recognizes downstream effectors. To address the mechanism of this intriguing and fundamental phenomenon, we have determined three-dimensional structures of active forms of the α subunit of G_{i1} by x-ray crystallography. The structures presented include those of the active forms of $G_{i\alpha 1}$ containing the bound nonhydrolyzable GTP analog, guanosine 5′-O-3-thiotriphosphate (GTPγS) (to 2.0 Å resolution), the active GDP·AlF_4^--bound complex (to 2.2 Å resolution), and two mutants with severely impaired guanosine triphosphatase (GTPase) activity—Arg^{178}→Cys $G_{i\alpha 1}$ and Gln^{204}→Leu $G_{i\alpha 1}$ (both to 2.3 Å resolution).

The 40.3-kD α subunit of G_{i1} is expressed widely but is particularly abundant in the brain (*4*). The native protein, which is bound at the cytoplasmic surface of the plasma membrane, is both myristoylated and palmitoylated at its amino terminus (*5*); myristate forms an amide linkage with the amino-terminal glycine residue, while palmitate is in thioester linkage with the adjacent cysteine. In association with a high-affinity dimer of G protein β and γ subunits, the G_{i1} heterotrimer can interact with α_2-adrenergic and M_2-muscarinic cholinergic receptors, among many others (*3*). Dissociation of GDP from $G_{i\alpha 1}$ is slow (0.03 min^{-1}) (*6*), and it is almost undetectable from the heterotrimeric protein complex. Activation of the G protein, which requires exchange of GDP for GTP, is thus dependent on its interaction with cytoplasmic segments of a ligand-activated, heptahelical receptor. This interaction is presumed to promote a transient "open" conformation of the α subunit from which GDP can dissociate and to which high cytosolic concentrations of GTP can bind. Mg^{2+} is very tightly associated with GTP and G_α in this complex (nanomolar affinity) and is required for activation of the α subunit and for subsequent hydrolytic activity (*7*). Mg^{2+}- and GTP-induced conformational changes result in dissociation of G_α from both the receptor and the βγ dimer, and both GTP-G_α and βγ are thereby freed to interact with and regulate downstream effectors (*8*). The best characterized effectors that are regulated by members of the $G_{i\alpha}$ subfamily are distinct isoforms of adenylyl cyclase. Types V and VI adenylyl cyclase are particularly susceptible to inhibition by $G_{i\alpha 1}$ (*9*). Slow hydrolysis of GTP (k_{cat} = 2 to 4 min^{-1} at 20°C) (*6*) returns $G_{i\alpha 1}$ to the GDP-bound species, which dissociates from effectors and associates again with βγ.

G_α subunits are poor catalysts, yet many of them exhibit rates of hydrolysis of GTP that are 100 or more times faster than the basal rates of hydrolysis catalyzed by their $p21^{ras}$ homologs. The GTPase activities of many $p21^{ras}$-like proteins and of certain G protein α subunits (but perhaps not $G_{i\alpha 1}$) can be stimulated by GTPase-activating proteins (GAPs) to rates of approximately 100 min^{-1} (*10*). By analogy with EF-Tu and $p21^{ras}$ (*11*), hydrolysis of GTP by G_α subunits probably occurs by an S_N2 in-line attack of a water molecule on the γ phosphate of the nucleotide. However, the mechanism by which these enzymes catalyze GTP hydrolysis has been elusive despite a wealth of crystallographic and mutagenic data. Much attention has been focused on a catalytic-site Gln residue (Gln^{61} in $p21^{ras}$; Gln^{204} in $G_{i\alpha 1}$), which is present in most GTPases (with a notable exception of EF-Tu, which contains His at this site) and an Arg residue (Arg^{178} in $G_{i\alpha 1}$; Arg^{174} in $G_{t\alpha}$), which occurs in all members of the heterotrimeric G_α family. Mutations at either of these sites largely abolish hydrolytic activity and thus stabilize the active, GTP-bound state (*12*). These mutations are of particular interest because Gln^{61} mutations in $p21^{ras}$ are a common cause of cellular transformation (*13*), and mutations at either of these sites in $G_{s\alpha}$ and $G_{i\alpha}$ are associated with human endocrine tumors, particularly of the pituitary (*14*).

In $p21^{ras}$, Gln^{61} has been postulated either to polarize (*15*) or orient (*16*) the hydrolytic water for attack on the γ phosphate or, alternatively, to stabilize the pentacoordinate transition state (*17*). However, these hypotheses are based on results obtained from crystallographic views of protein complexes with nonhydrolyzable analogs of GTP, mutagenesis of the protein, or molecular dynamics simulations, and transition-state complexes have not been observed. The three-dimensional structure of GTPγS-$G_{t\alpha}$ reveals that Arg^{174} is hydrogen-bonded to the sulfur atom of the γ thiophosphate moiety, the bridging oxygen between the β and γ phosphates, and a nonbridging oxygen on the α phosphate (*18*). Such stabilization of the ground state does not offer obvious insight into the biochemical characteristics of proteins with mutations at this Arg residue; these proteins appear to bind guanine nucleotides normally despite their inability to hydrolyze GTP. Cholera toxin catalyzes the adenosine diphosphate (ADP)–ribosylation of the corresponding Arg residue in $G_{s\alpha}$ (Arg^{201}) and $G_{t\alpha}$ (Arg^{174}) (*19*), which also results in abolition of hydrolytic activity (*20*).

The first three authors contributed equally to this work. D. E. Coleman, A. M. Berghuis, and S. R. Sprang are with the Howard Hughes Medical Institute and the Department of Biochemistry, and E. Lee, M. E. Linder, and A. G. Gilman are in the Department of Pharmacology, The University of Texas Southwestern Medical Center, Dallas, TX 75235, USA.

*Present address: Department of Cell Biology and Physiology, Washington University School of Medicine, St. Louis, MO 63108, USA.

†To whom correspondence should be addressed.

Table 1. X-ray data collection. Crystals of $G_{i\alpha 1}$ were grown and prepared for x-ray data collection as described (*24, 25*). Data sets for crystals of the native protein and the uranyl derivatives were collected at the F1 beamline at the Cornell High Energy Synchrotron Source (CHESS). The data set for $Gln^{204}\rightarrow Leu$ $G_{i\alpha 1}$ was collected at the CHESS F2 beamline. Both beamlines were equipped with Fuji imaging plate detector systems. The $Arg^{178}\rightarrow Cys$ $G_{i\alpha 1}$ and native GDP·AlF_4^-–$G_{i\alpha 1}$ data sets were collected with an R axis–II imaging plate system with an RU300 x-ray generator. The selenomethionyl GTPγS-$G_{i\alpha 1}$ multiwavelength anomalous dispersion (MAD) data were collected from two crystals using the inverse beam method at the Howard Hughes Medical Institute X4a beamline at the National Synchrotron Light Source (NSLS) equipped with a Fuji imaging plate system. Wavelengths were calibrated with EXAFS scans of selenomethionyl GTPγS-$G_{i\alpha}$ protein crystals and selenium foil standards. All data were integrated and scaled by means of the DENZO/SCALEPACK (*46*) package. Only full reflections were used for the Fuji image plate data. The selenomethionyl GTPγS-$G_{i\alpha 1}$ MAD data were also processed by the scaling procedure of the MADSYS (*47*) MAD data processing package.

Data set	Beam	λ (Å)	*T*	Total obs.	Redundancy	Completeness (%)	Resolution (Å)	R_m*	⟨*I*/σ⟩
Native GTPγS	CHESS F1	0.910	7°C	58,811	2.3	92.7	20–2.0	0.058	12.1
$Arg^{178}\rightarrow Cys$	R axis–II	1.542	100 K†	40,514	2.5	93.7	15–2.3	0.049	13.6
$Gln^{204}\rightarrow Leu$	CHESS F2	1.079	100 K†	58,697	3.3	97.2	15–2.3	0.041	20.2
Native GDP·AlF_4^-	R axis–II	1.542	100 K†	96,580	4.9	97.8	15–2.2	0.053	15.3
$K_3UO_3F_5$	CHESS F1	0.910	7°C	42,928	2.1	97.1	20–2.2	0.078	6.4
$UO_2(NO_3)_2$	CHESS F1	0.910	7°C	21,968	1.9	78.8	20–2.5	0.050	16.5
Selenomethionyl	NSLS	0.9879	108 K‡	40,331	3.2	86.1	20–2.5	0.046	22.2
GTPγS MAD data	(X4A)	0.9802		37,644	3.0	84.0	20–2.5	0.057	19.7
		0.9800		34,821	2.9	82.4	20–2.5	0.061	18.6
		0.9705		35,155	2.9	82.0	20–2.5	0.056	18.5

*$R_m = \frac{\Sigma|I - \langle I\rangle|}{\Sigma\langle I\rangle}$, all values from SCALEPACK. †Molecular Structure Corporation Cooling System. ‡Oxford Cryostream cooling system.

The architecture of $G_{i\alpha 1}$, presented below, is similar to that of the closely related α subunit of G_t (*18*). Nevertheless $G_{i\alpha 1}$ and $G_{t\alpha}$ are activated by different receptors, interact preferentially with different species of βγ, and regulate different effectors. Comparison of the structures of the two molecules and ultimately their complexes with their molecular partners should reveal the structural elements that have diverged to enable these two proteins to engage in distinct sets of regulatory interactions. Of the structures that we present, perhaps the most surprising and illuminating is that of $G_{i\alpha 1}$ complexed with GDP and AlF_4^-. The AlF_4^- is an activator of GDP-bound G protein α subunits because, as has been suggested, of the anion's capacity to substitute for and mimic the γ-phosphate of GTP (*21*). In fact, the x-ray structure reveals GDP·AlF_4^- to be a transition state analog.

Structure determination. The structure of $G_{i\alpha 1}$ was ultimately determined by molecular replacement with the coordinates for the GTPγS-$G_{t\alpha}$ complex as a search model (*18*). Prior to this, two isomorphous uranyl derivatives of GTPγS-$G_{i\alpha 1}$ had been identified, and a complete multiwavelength anomalous data set had been measured from crystals of selenomethionyl GTPγS-$G_{i\alpha 1}$ to be used for multiwavelength anomalous dispersion (MAD) phasing (*22*). Although these data were not used to develop the initial model, they provided independent phase information, which proved useful in the structural analysis.

Nonacylated, full-length $G_{i\alpha 1}$ and the $Arg^{178}\rightarrow Cys$ and $Gln^{204}\rightarrow Leu$ mutants of $G_{i\alpha 1}$ were synthesized in *Escherichia coli* and purified (*23*). The yield of purified protein was approximately 40 mg per liter of bacterial culture. Crystallization of wild-type and mutant GTPγS-$G_{i\alpha 1}$ complexes has also been described (*24*). Crystals of GDP·AlF_4^--$G_{i\alpha 1}$ and selenomethionyl GTPγS-$G_{i\alpha 1}$ were obtained under similar conditions (*25*). Two uranyl derivatives were prepared from native crystals; both share a single, common site. X-ray data were measured and processed as described (Table 1). Complete data sets for the selenomethionyl derivative were measured to a resolution limit of 2.5 Å at four wavelengths: one above and one below the selenium 12.6540 keV K absorption edge and the other two corresponding to the energy maxima for the real and imaginary components of anomalous scattering.

The structure of GTPγS-$G_{i\alpha 1}$, determined by molecular replacement (*26*), is now refined to a crystallographic *R* factor of 0.175 at a limiting resolution of 2.0 Å (Table 2). A volume of the electron density map computed with phases from the refined model is shown in Fig. 1A. As a guard against model bias, an electron density map was also computed with phase information derived from the single isomorphous uranyl derivative and from selenium anomalous scattering. Positions of the methionine sulfur atoms from the refined model were used to compute the anomalous phase contribution (Table 3). The resulting electron density map (Fig. 1B) corresponds well with the refined model.

The asymmetric unit contains one subunit of $G_{i\alpha 1}$. The refined model comprises residues 34 to 343 (of 353 residues present in the molecule; the amino-terminal Met is cleaved), the bound Mg^{2+}·GTPγS

Table 2. Refinement statistics.

Data set	Resolution (Å)	Reflections* (*N*)	*R* factor† (%)	*R* free‡ (%)	Atoms (*N*)	Waters (*N*)	Deviation from ideality (rms)		rms deviation of Cα's versus native GTPγS-$G_{i\alpha 1}$, (Å)
							Bonds (Å)	Angles (°)	
Native GTPγS	8–2.0	22,440	17.5	22.8	2650	126	0.010	1.381	—
$Arg^{178}\rightarrow Cys$ GTPγS	8–2.3	14,535	21.7	28.0	2573	77	0.011	1.501	0.506
$Gln^{204}\rightarrow Leu$ GTPγS	8–2.3	14,544	23.0	31.0	2561	52	0.013	1.588	0.502
Native GDP·AlF_4^-	8–2.2	17,407	22.2	28.2	2594	93	0.012	1.505	0.672

*$F/\sigma > 1.0$ reflections used for refinement after random removal of 10 percent of reflections for use in *R* free calculation (*41*). †*R* factor = $\Sigma|F_o - F_c|/\Sigma F_o$ where F_o and F_c are the observed and calculated structure factor amplitudes of the reflections used for refinement. ‡*R* free = *R* factor for the set of reflections removed prior to refinement and used to monitor the reliability of the refinement.

complex, and 126 ordered solvent molecules. More than 95 percent of the nonglycine residues exhibit Φ and ψ torsion angles within the "most favorable" regions of the Ramachandran plot (*27*). None adopt disallowed conformations.

Crystals of Gln^{204}→Leu GTPγS-$G_{i\alpha1}$ and Arg^{178}→Cys GTPγS-$G_{i\alpha1}$ and that of the GDP·AlF_4^--$G_{i\alpha1}$ complex are isomorphous with the wild-type crystals. X-ray data for the Arg^{178}→Cys and Gln^{204}→Leu mutants and the GDP·AlF_4^- complex were measured and processed (Table 1). Structural changes were examined in difference Fourier maps. Modified GTPγS-$G_{i\alpha1}$ structures were used as starting models subjected to crystallographic refinement (*26*) (Table 2).

Molecular architecture; recognition of effectors and βγ subunits. $G_{i\alpha1}$ is constructed from two domains: a $p21^{ras}$-like αβ domain flanked by an α helical (helical) module that is common to G_α subunits. The fold of the molecule is identical to that of $G_{t\alpha}$ (Fig. 2, A and B) (*18*); the two molecules can be superimposed with a root mean square deviation (rms) of 1.2 Å at Cα positions. This rather large deviation, given the 68 percent sequence identity between the two molecules, can be attributed to both local and global differences between the structures. The most noteworthy of these is apparent in the conformation of residues 108–120, which correspond to the terminus of helix B and the connecting loop to the following helix C (Fig. 2B). [Secondary structural elements are named according to the convention developed for $p21^{ras}$ and extended by Noel *et al.* (*18*).] The αB helix terminates at residue 109 in $G_{t\alpha}$ (residue 113 in $G_{i\alpha1}$), but in $G_{i\alpha1}$ it is slightly kinked by a 3_{10} turn and then continues for an additional turn of α helix to residue 116. This structural difference might be attributed to the replacement of a pair of residues in close van der Waals contact—Met^{106} and Met^{119} in $G_{t\alpha}$—with Leu^{110} and Leu^{123} in $G_{i\alpha1}$. The reduction in packing volume apparently allows helix B to continue for an additional four residues and results in a more compact interface between the B and C helixes.

Experiments with chimeras of human and *Xenopus* $G_{s\alpha}$ suggest that stimulation of adenylyl cyclase activity by these proteins might require residues in a segment corresponding to $G_{s\alpha}$ (short form) 70–140 (*28*). The human and *Xenopus* sequences, which are 92 percent identical, differ by six residues within the sequence 118–128, which corresponds almost exactly to the region in $G_{i\alpha1}$ (110–120) that exhibits the largest structural deviation from $G_{t\alpha}$. This is also a region of general sequence divergence among G_α subunits. On this basis we think that the helical domain, and in particular the helix B–helix C region, may be an effector binding site, even though this portion of the molecule is spatially distant from other known regions of G_α effector contact. Preliminary crystallographic analysis of crystals of $G_{i\alpha1}$ grown in the presence of GDP (*24*) indicates that substantial structural changes occur in the helix B–helix C segment upon GTP hydrolysis (*29*).

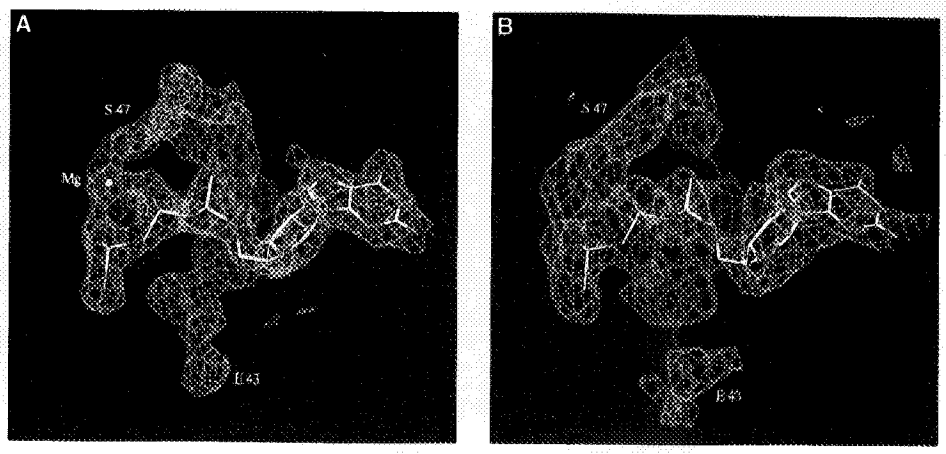

Fig. 1. Electron density maps drawn with the Program O (*40*) in the vicinity of the GTPγS binding site in $G_{i\alpha1}$. (**A**) The $2F_o - F_c$ map contoured at 2σ, computed with 8 to 2.0 Å data with phases from the refined atomic model. (**B**) F_o map contoured at 1σ, computed with single isomorphous replacement and MAD phases. Carbon and phosphorous atoms are colored yellow; nitrogens, blue; oxygens, red; and sulfur atoms green.

Comparison of $G_{t\alpha}$ and $G_{i\alpha1}$ suggests that the helical and $p21^{ras}$-like domains behave to a first approximation as rigid units connected by two flexible tethers, one of which (linker 2, residues 177–183) forms part of the nucleotide binding site. The helical and $p21^{ras}$-like domains of $G_{i\alpha1}$ and $G_{t\alpha}$, when superimposed independently, correspond more closely than do the entire proteins (Fig. 2B). The same analysis shows that, on superimposing the helical domains of $G_{i\alpha1}$ and $G_{t\alpha}$, the $p21^{ras}$-like domain of $G_{i\alpha1}$ must be rotated 3.5° toward the helical domain to bring it into correspondence with the $p21^{ras}$-like domain of $G_{t\alpha}$. Since the axis of this pseudo-rotation is close to the GTP binding site in the center of the molecule, the substrate binding pockets of the two α subunits are almost identical. The more open conformation of the $G_{i\alpha1}$ subunit relative to $G_{t\alpha}$ may reflect its complementarity to a different effector (in that binding sites for effectors might reside on both the $p21^{ras}$-like and helical domains) or simply the variation expected for rigid domains connected by flexible hinges.

Although the $G_{i\alpha1}$ protein present in the crystals is intact, no electron density is observed for either the amino-terminal 32 residues or the carboxyl-terminal 11 residues. It is unlikely that there is bias from the search model of $G_{t\alpha}$ (where the amino terminus is proteolytically cleaved), since density is also absent from maps computed with combined single isomorphous replace-

Table 3. Phasing statistics. Heavy atom sites were refined in MLPHARE (*48*) as implemented in CCP4 (*49*). In this procedure the diffraction data from the selenomethionyl GTPγS-$G_{i\alpha1}$ crystal collected at different wavelengths were treated as separate derivatives. Wavelength 3 (0.9800 Å) was used as the native data set, explaining the absence of phasing power and centric and acentric Cullis *R* factors for this set. By combining the phase information from both the uranyl derivatives and the MAD experiment, an overall figure of merit of 0.60 for all data between 15.0 and 2.8 Å was obtained. The correlation coefficient for the map calculated using these phases with that of the final [$2F_o - F_c$ electron density map] was 0.476.

Derivative	Phasing power		Cullis *R* factor			Occ.*	Δ*F*/*F*†
	Acent.	Cent.	Acent.	Cent.	Anom.		
$UO_2(NO_3)_2$	1.0	0.6	0.75	0.82	----	0.56	0.179
$K_3UO_3F_5$	0.8	0.5	0.80	0.86	1.00	0.44	0.185 (0.072)
Se λ_1 = 0.9879	0.7	0.7	0.88	0.70	1.00	—	0.052 (0.048)
Se λ_2 = 0.9802	0.2	0.2	0.99	0.96	1.00	—	0.043 (0.072)
Se λ_3 = 0.9800	—	—	—	—	0.60	—	— (0.087)
Se λ_4 = 0.9705	0.7	0.7	0.88	0.70	0.70	—	0.058 (0.073)

*The two uranyl derivatives both contained one common site at $x = 0.756$, $y = 0.316$, $z = 0.055$, $B = 26$ Å^2, which was determined by inspection of difference Patterson maps. The initial positions of the selenium atoms were taken from the final refined model of GTPγS-$G_{i\alpha1}$. †$\Delta F/F = \Sigma|F_{nat} - F_{der}|/\Sigma F_{nat}$; the values given in parentheses refer to the anomalous component of the scattering factor and is defined as $\Delta F/F = \Sigma|F^+ - F^-|/\Sigma F$.

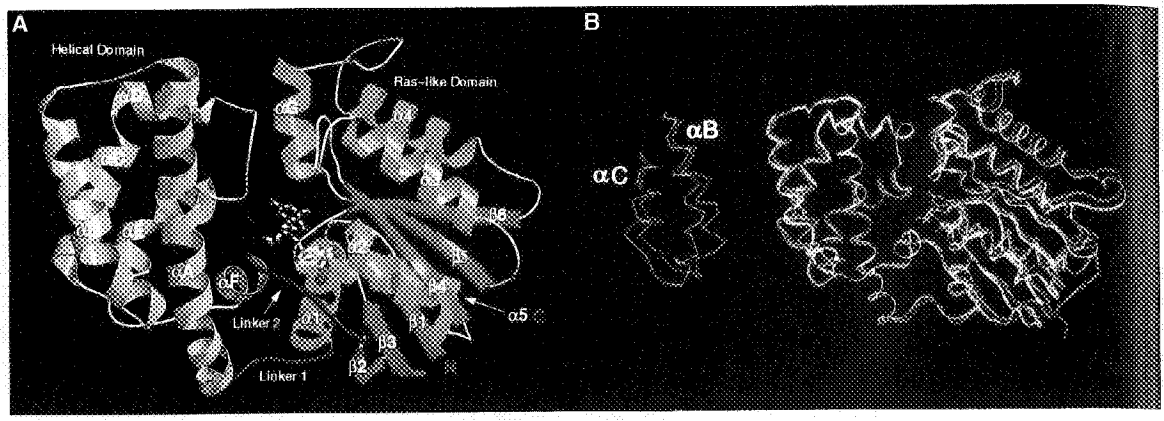

Fig. 2. (**A**) Ribbon and coil schematic of $G_{i\alpha 1}$ subunit. The helical domain is colored yellow, and the p21^{ras}-like domain is green and cyan. Linker 1 and linker 2 strands are colored red. The GTPγS is shown as a ball and stick model, and the magnesium ion is depicted as a magenta sphere. Secondary structure elements are labeled. The red N and C mark the positions of the first ordered residues at the amino and carboxy termini of the molecule. The image was computed with the program MOLSCRIPT (*42*) and rendered with RASTER3D (*43*). (**B**) A superposition of $G_{i\alpha 1}$ (cyan) with $G_{t\alpha}$ (red) using the C_α atoms of residues 62–107 ($G_{i\alpha 1}$ numbering) and 120–182 of the helical domain and linker 2 peptide. The rms deviation of the atoms used in this superposition is 0.77 Å. Superposition of residues 33–54 and 183–343 of the p21^{ras} domain yields an rms deviation of 0.63 Å. The insert (left) shows the superimposed αB–αC loops of $G_{i\alpha 1}$ and $G_{t\alpha}$, rotated by about 90° about the vertical axis, from the full view shown on the right.

ment and MAD phases, which contain no model information. The observed disorder of the amino and carboxyl termini may be functionally significant. A wide variety of experimental evidence indicates that the amino terminus participates in βγ binding, whereas the carboxyl terminus participates in receptor recognition (*30*). Disorder in these regions may account for the weak affinity of the GTP-bound form of the α subunit for both the βγ subunit complex and the intracellular domains of heptahelical receptors. Hydrolysis of GTP may induce the amino terminus to adopt an ordered conformation, allowing it to form part of the βγ binding surface.

Guanine nucleotide binding. The nucleotide is buried in the cleft between the helical and the p21^{ras}-like domains of the G_α subunit, although all of the direct contacts are formed with either the domain linker peptide 2 or the p21^{ras}-like domain itself (Fig. 3). Therefore, all of the nucleotide binding elements have structural homologs in p21^{ras} and EF-Tu. The α and β phosphates of GTPγS are firmly tethered to residues in the β1-α1 loop (residues 45–48), whereas the γ thiophosphate group forms hydrogen bonds to residues in the β3-α2 connector (residues 201–203) and the linker 2 peptide. These segments also contribute to the octahedral coordination sphere of the magnesium ion, similar to that seen in p21^{ras}, with the β and γ phosphates providing two oxygen ligands; the remaining oxygen atoms are donated by the side chains of Ser^{47} and Thr^{181} and by two water molecules. Asp^{200} (not shown in Fig. 3A) is likewise conserved in the second coordination sphere. The structure of the GDP-$G_{t\alpha}$ complex (*31*) shows that the linker 2 (switch I) and β3-α2 (switch II) segments that bind the γ phosphate and Mg^{2+} are perturbed on hydrolysis of GTP, but that the β1–α1 loop, which interacts with the α and β phosphates, remains undisturbed.

Both p21^{ras} and G protein α subunits bind GTP with nanomolar affinity. Although the helical domain of $G_{i\alpha 1}$ shields the nucleotide from solvent, it does not appear to contribute any additional binding energy to the GTP complex. Two pairs of ionically bonded residues, Asp^{150}·Lys^{270} and Arg^{178}·Glu^{43}, arch over the interdomain cavity and trap the nucleotide within (Fig. 3B). Although most of the protein-nucleotide interactions are directly analogous to those observed in p21^{ras} (*15*, *32*), the two proteins adopt somewhat different mechanisms for supporting the purine ring of the guanine nucleotide. In p21^{ras}, Phe^{28}, located in the β1–β2 loop, performs this function. Leu^{175}, its homolog in $G_{i\alpha 1}$, is part of the linker 2 segment that connects the p21^{ras}-like and helical domains, and it is not located in the GTP binding site. Instead, Thr^{327} downstream of the β6 strand buttresses the guanine ring in a manner analogous to that of Phe^{28} in p21^{ras}. As in p21^{ras} and EF-Tu, the exocyclic-ring oxygen atoms of the nucleotide ribose moiety accept hydrogen bonds from the backbone carbonyl oxygens of residues 175 and 176 in the linker 2 strand. The two water-mediated hydrogen bonds linking the ribose 3′ hydroxyl and the guanine

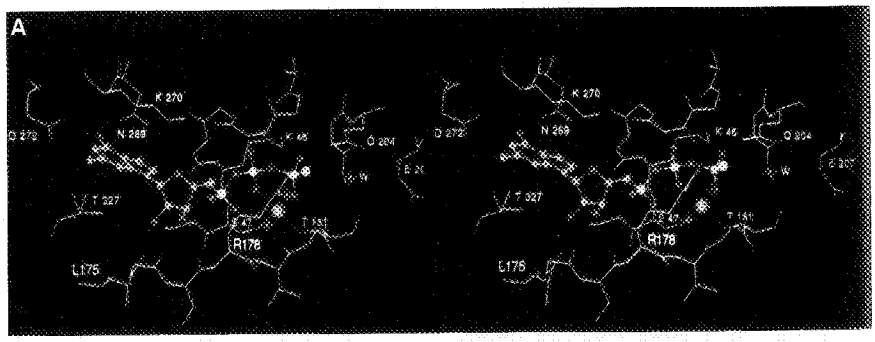

Fig. 3. Binding site of GTPγS. (**A**) Stereo view. Coloring scheme: carbon (GTPγS), green; carbon (protein), orange; nitrogen, blue; oxygen, red; sulfur and phosphorus, yellow; and magnesium, magenta. Water molecules belonging to the coordination sphere of the magnesium and the putative water nucleophile (W) are shown. Sphere radii are not drawn in proportion to atomic radii. (**B**) This view, rotated approximately 90° about the vertical axis of Fig. 3A, shows carbon atoms from the helical and linker 2 domains in white. Side chain interactions trap the nucleotide between p21^{ras}-like and helical domains.

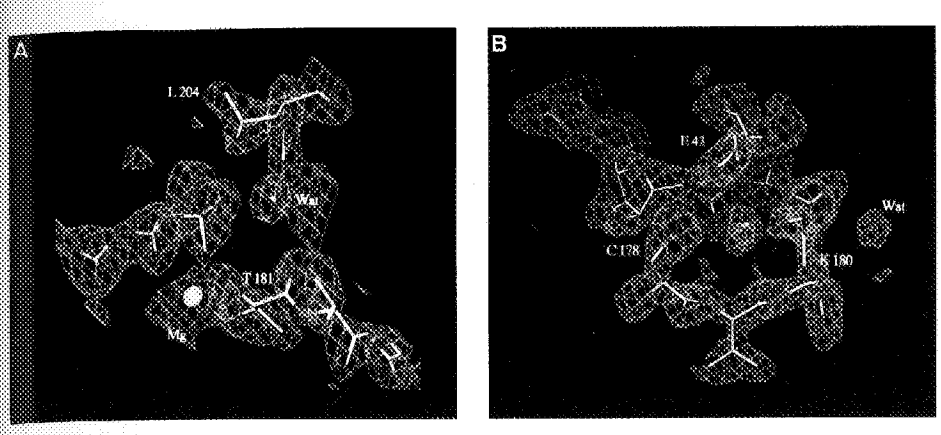

Fig. 4. $2F_o - F_c$ electron density maps contoured at 1.5σ, computed with refined phases (Table 2) to 2.3 Å resolution, at the GTPγS binding sites: (**A**) GTPγS-Gln^{204}→Leu $G_{i\alpha1}$ (**B**) GTPγS-Arg^{178}→Cys $G_{i\alpha1}$; the putative water nucleophile is present in the active site of both complexes.

N3 to Ser^{151} are the only interactions between the nucleotide and the helical domain.

There are only two significant differences between the nucleotide binding sites of $G_{i\alpha1}$ and $G_{t\alpha}$. The Leu at position 273 in $G_{i\alpha1}$ is replaced by Val in $G_{t\alpha}$, which is the only substitution within 4.5 Å of the nucleotide. The larger side chain in $G_{i\alpha1}$ is in van der Waals contact with Asp^{150} and excludes a water molecule that is found between the corresponding two residues in $G_{t\alpha}$. Asp^{150} is shifted toward Leu^{273}, thus filling the cavity occupied by the water in $G_{t\alpha}$.

Of more direct relevance to the mechanism of nucleotide binding and hydrolysis is the conformation of Arg^{178} which, in $G_{t\alpha}$, is in contact with the α and β phosphates as well as the sulfur of the nucleotide analog (*18*). In contrast, the side chain of Arg^{178} is poorly ordered in $G_{i\alpha1}$ (B = 39 Å^2; B/B_{ave} = 2.0) (*33*) and forms no contacts with the nucleotide. Instead, the plane of the guanidinium moiety is parallel to and displaced by 3.0 Å from that of the carboxylate group of Glu^{43} (Fig. 3B).

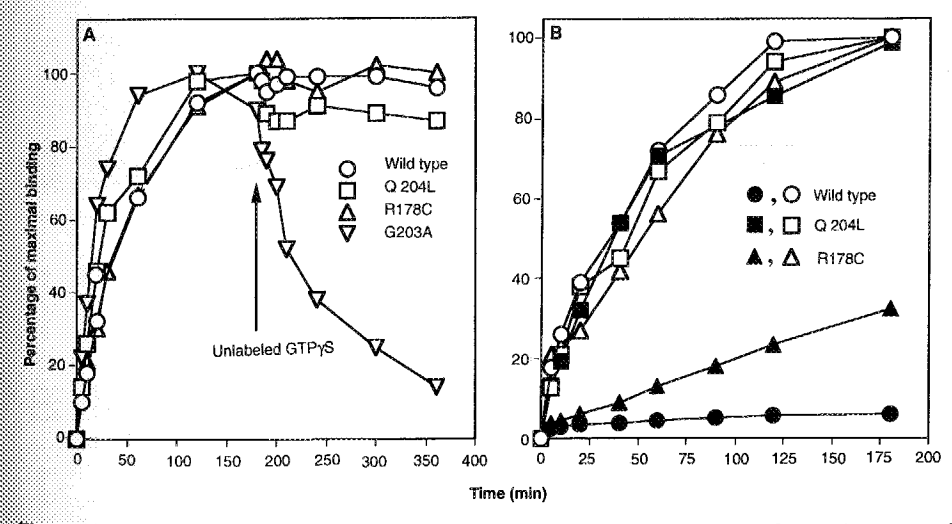

Fig. 5. (**A**) Kinetics of [^{35}S]GTPγS association with and dissociation from wild-type $G_{i\alpha1}$ and mutants of $G_{i\alpha1}$. Proteins (10 μg/ml) were incubated at 30°C in 100 mM Hepes (sodium salt) (pH 8.0), 1 mM EDTA, 10 mM DTT, 10 mM $MgSO_4$, and 2 μM [^{35}S]GTPγS (700 cpm/pmol). After 180 minutes, 100 μM unlabeled GTPγS was added to initiate exchange of labeled for unlabeled nucleotide. Samples were withdrawn at the indicated times and analyzed (*44*) for bound, ^{35}S-labeled nucleotide. Values are expressed as a percentage of the maximal value observed for each protein. Reactions were performed with wild-type $G_{i\alpha1}$ (○), Gln^{204}→Leu $G_{i\alpha1}$ (□), and Arg^{178}→Cys $G_{i\alpha1}$ (△). Gly^{203}→Ala $G_{i\alpha1}$ (▽) was also included because GTPγS is known to dissociate from this mutant protein (*45*). (**B**) Effect of AlF_4^- on GTPγS binding to wild-type and mutant $G_{i\alpha1}$ proteins. The rate of GTPγS binding is limited by the rate of GDP dissociation. Proteins (10 μg/ml) were incubated at 30°C in 100 mM Hepes (sodium salt) (pH 8.0), 1 mM EDTA, 10 mM DTT, 2 mM $MgSO_4$, and 2 μM [^{35}S]GTPγS (2000 cpm/pmol). Reactions designated with filled symbols contained in addition 30 μM $AlCl_3$ and 10 mM NaF. Samples were withdrawn at the indicated times and analyzed as described (*44*) for bound, ^{35}S-labeled nucleotide. Values are expressed as a percentage of the maximal value observed for each protein in the absence of AlF_4^-. Reactions were performed with wild-type $G_{i\alpha1}$ (○, ●), Gln^{204}→Leu $G_{i\alpha1}$ (□, ■), and Arg^{178}→Cys $G_{i\alpha1}$ (△, ▲).

The mechanism of GTP hydrolysis. Because members of the G protein–p21^{ras} superfamily are poor catalysts, it has been difficult to discern the mechanism of GTP hydrolysis. Potential catalytic ligands might be expected to orient the nucleophilic water or activate it by polarization or proton abstraction. Other residues might be expected to stabilize the developing negative charge about the γ phosphate or to protonate the leaving group. The tightly coordinated Mg^{2+} is absolutely required, and its role in catalysis has been discussed (*1*, *34*). As in the structures of EF-Tu (*35*), p21^{ras} (*32*, *34*), and $G_{t\alpha}$ (*18*) complexed with GTP analogs, a candidate for the attacking water molecule appears in the expected axial position of the GTPγS-$G_{i\alpha1}$ complex, 3.85 Å from the γ phosphate (Fig. 3A). Barring a major conformational change at the catalytic center, Gln^{204} and Glu^{207} appear to be the only residues capable of interacting directly with the putative nucleophilic water molecule.

The role of the conserved and apparently essential Gln^{204} residue in catalysis has been elusive. In GTPγS-$G_{i\alpha1}$, the Gln^{204} side chain forms no hydrogen bonds or short (≤3.5 Å) van der Waals contacts, nor is it in contact with any ordered solvent molecules. The average thermal parameters for the side chain atoms are relatively high (B = 38 Å^2; B/B_{ave} = 1.9), although the main-chain atoms are well ordered.

Replacement of Gln^{204} by Leu in $G_{i\alpha1}$ does not perturb the active site or the binding mode of the nucleotide (Fig. 4A). The presumptive nucleophilic water molecule remains bound. Similar results were obtained by Privé *et al.* (*17*) in their crystallographic analysis of the Gln^{61}→Leu p21^{ras} oncogene product. The crystallographic data are consistent with measurements of the rates of association of GTPγS with $G_{i\alpha1}$ (which is limited by and therefore equal to the rate of dissociation of GDP) and dissociation of GTPγS from the protein, which indicate that the affinities of Gln^{204}→Leu $G_{i\alpha1}$ for substrate and product are similar to those of the wild-type protein (Fig. 5A). We infer that Gln^{204} does not contribute substantially to the binding of GTP or the attacking water molecule in the ground-state E·S complex. Rather, we believe that Gln^{204} exerts its influence in the transition state, as described below.

Likewise, Arg^{178} forms no direct contacts with GTPγS in $G_{i\alpha1}$, although its side chain is poised over the triphosphate moiety of the nucleotide. The structure of the Arg^{178}→Cys mutant complex (Fig. 4B) is essentially identical to that of the wild type, again indicative of the fact that the Arg residue does not participate in ground-state stabilization. This is further substantiated by observation of unperturbed rates of dis-

sociation of GTPγS and GDP from Arg^{178}→Cys $G_{i\alpha1}$ (Fig. 5A).

The roles of Arg^{178} and Gln^{204} are strikingly revealed in the structure of the GDP·AlF_4^- complex with $G_{i\alpha1}$. Rearrangement of these residues and the structure of the GDP·AlF_4^- moiety suggest that this complex mimics the transition state of the S_N2 reaction. The 2.2 Å electron density map shows the nucleotide and the AlF_4^- as well defined and discrete entities, with AlF_4^- occupying the position normally filled by the γ phosphate of GTP (Fig. 6A). However, in contrast to the tetrahedral geometry of a phosphate group, AlF_4^- forms a square planar complex that is octahedrally coordinated to a β-phosphate oxygen and to a putative water molecule as the trans axial ligands (Fig. 6, A and D). The axial water molecule appears in a position near that of the putative hydrolytic water seen in the GTPγS-bound structures, but it is shifted by 1.5 Å toward the aluminum. The position and coordination sphere of the Mg^{2+} are identical to that seen in the Mg^{2+}·GTPγS complex except in that a fluoride atom (F3, Fig. 6D) substitutes for an oxygen atom of the GTP γ phosphate. The loop (182–186) connecting linker 2 with the β4 strand has shifted by up to 1.4 Å toward helix B. This might occur as a consequence of a rotation of Thr^{181} which is coupled by hydrogen bonding to the translation of the water nucleophile toward the aluminum ion. Otherwise, the GDP·AlF_4^- $G_{i\alpha1}$ structure is identical to that of the GTPγS bound form. This is consistent with the ability of GDP·AlF_4^- complexes of G proteins to interact with effectors.

The dramatic reorientations of Arg^{178} and Gln^{204} induced by GDP·AlF_4^- provide compelling evidence for their roles in catalysis (Fig. 6, B and C). The side chain of Arg^{178} moves further into the active site and forms hydrogen bonds with two of the fluoride atoms (F1 and F2, Fig. 6, C and D), displacing a water molecule found in the GTPγS structure; it also interacts with the α and β phosphate oxygens of GDP. The side chain of Gln^{204} rotates to bring it into hydrogen bonding contact with both a fluoride atom (F1) and the axial water molecule (36). The side chains of both Gln^{204} and Arg^{178} are immobilized by contact with AlF_4^-, which is evident from the electron density (Fig. 6A) and the refined thermal parameters (Arg^{178}, B = 11.78 $Å^2$, B/B_{ave} = 0.6; Gln^{204}, B = 27.03, and B/B_{ave} = 1.3). It thus appears that these two residues are mobile and do not bind substrates in the ground state but interact tightly with both substrates (GTP and the nucleophilic water) in the transition state.

The affinity of AlF_4^- for GDP-$G_{i\alpha1}$ can be inferred from the effect of AlF_4^- on the rate of dissociation of GDP from the protein (which is measured simply by examination of the rate of [^{35}S]GTPγS binding). Addition of AlF_4^- substantially slows the rate of dissociation of GDP from wild-type $G_{i\alpha1}$, while having a lesser effect on the Arg^{178}→Cys mutant and virtually no effect on Gln^{204}→Leu $G_{i\alpha1}$ (Fig. 5B). These data are consistent with the structural observations that these two residues participate in stabilization of the GDP·AlF_4^-–$G_{i\alpha1}$ complex (Fig. 5B) but not the GTPγS-$G_{i\alpha1}$ complex (Fig. 5A).

Aluminum fluoride does mimic the γ phosphate of GTP by promoting an active conformation. However, the geometry and coordination of the GDP·AlF_4^- complex, the structural changes within the catalytic

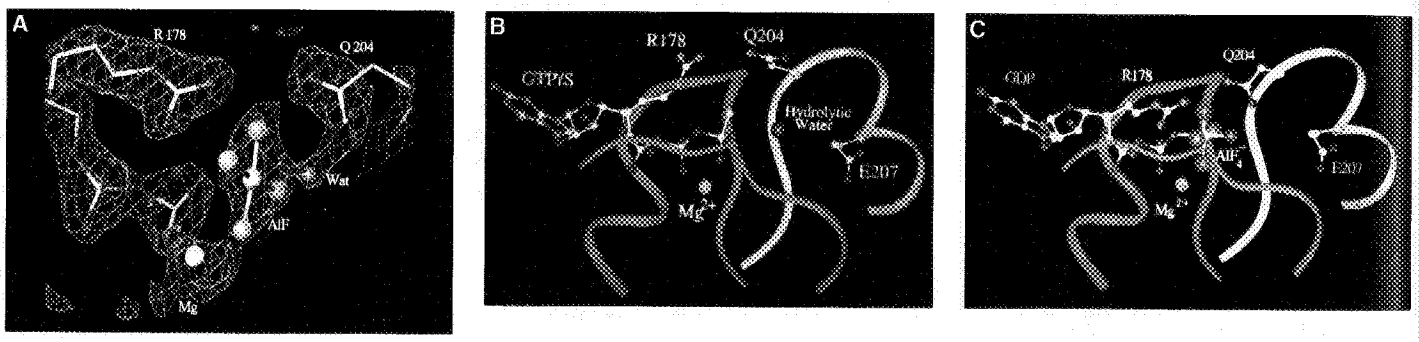

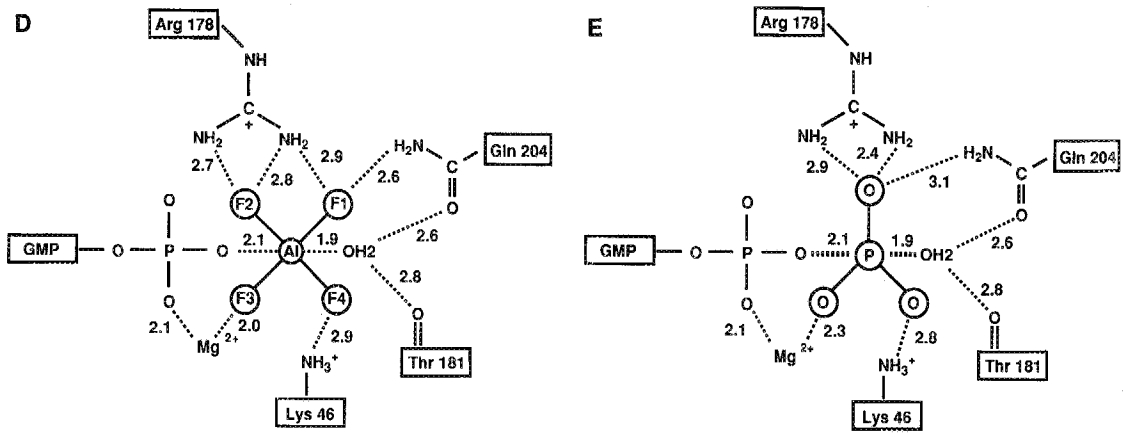

Fig. 6. The GDP·AlF_4^- complex of $G_{i\alpha1}$. (**A**) $2F_o - F_c$ electron density map contoured at 1.5σ, computed with refined phases (Table 2) to 2.2 Å resolution. The aluminum atom is colored brown, the fluorides green, and magnesium yellow. (**B**) A schematic of the active site in the GTPγS complex, showing the disposition of Arg^{178} and Gln^{204}; these residues are not within hydrogen bonding distance of the nucleotide. The putative water nucleophile is positioned 3.85 Å from the γ phosphorus trans axial to the βγ, bridging phosphate oxygen atom. The β1–α1 loop is colored green, the β2–α3 switch peptide yellow, and the linker 2 strand is blue. (**C**) The GDP·AlF_4^- complex shown from the same perspective. Arg^{178} and Gln^{204} have rotated to contact the AlF_4^- cluster, and the nucleophilic water has moved into the ligand field of the aluminum ion. (**D**) Schematic showing the coordination sphere and contact distances (Å) of AlF_4^- involving Arg^{178}, Gln^{204}, the magnesium ion, and other active site residues. The average Al–F bond distance is 1.8 Å. (**E**) Model of the active site of $G_{i\alpha1}$ at the transition state of the phosphorolysis reaction, based on the structure of the GDP·AlF_4^- complex. The phosphorus atom of a trigonal "PO_3" group was centered on the aluminum ion of the AlF_4^- with the planes of the "PO_3" group coincident with that of AlF_4^-. P–O bond distances and the O–P–O angles were set to 1.65 Å and 120°, respectively. The PO_3 group was rotated to achieve a O–Mg distance similar to that observed for the F3–Mg contact in the AlF_4^- complex. This model is otherwise identical to the GDP·AlF_4^- complex.

site, and the guanine nucleotide exchange kinetics of the wild-type and mutant proteins all argue that GDP·AlF_4^- is not a GTP analog but rather mimics the trigonal-bipyramidal species presumed to appear at or near the transition state of the S_N2 reaction (Fig. 6E).

For these reasons, we propose that Arg^{178} promotes bond cleavage by stabilizing the developing negative charge on the equatorial oxygen atoms of the γ phosphate. A similar view was expressed by Noel *et al.* (*18*). The weak hydrolytic activity of the $p21^{ras}$ enzymes, which do not have an Arg residue at a position analogous to 178 and cannot be activated by AlF_4^-, suggests that Arg^{178} provides up to 2.5 kcal of energy to stabilize the transition state.

Extrapolating from the hydrogen bond coordination between Gln^{204} and the AlF_4^- complex (Fig. 6, C and D), we infer that Gln^{204} may stabilize the axial coordination of the nucleophilic water molecule to the trigonal γ phosphate in the transition state (Fig. 6E). The amide group of the Gln residue could serve as a hydrogen bond donor to the equatorial γ phosphate oxygen atoms, in analogy to the donation of a hydrogen bond to the negatively charged fluoride atoms of AlF_4^-. The axial water is consequently a hydrogen bond donor to both the carboxamide oxygen of Gln^{204} and the main-chain carbonyl of Thr^{181} (Fig. 6E). In the transition state, we propose that these ligands orient the lone pair orbitals of the nucleophilic water toward the developing positive charge on the γ phosphorus, and in their capacity as hydrogen bond acceptors, polarize the water for nucleophilic attack. A similar role for Gln^{61} was anticipated by model-building and molecular dynamics simulation of the transition state in $p21^{ras}$ by Privé *et al.* (*17*). A molecular dynamics simulation performed by Frech *et al.* (*16*) suggests that Gln^{61} might also contact the water nucleophile in the ground-state GTP complex (*37*).

Although Gln^{204} appears to have significant involvement in the transition state, it is unlikely that it serves as a general base. Insertion of a catalytic base at this position (for example, mutation of the equivalent Gln^{61} in $p21^{ras}$ to Glu) does increase k_{cat} by 20 times but results in an even larger increase in K_m, presumably because of introduction of a negative charge so close to the γ phosphate (*16*). Noel *et al.* (*18*) have proposed that a neighboring conserved Glu residue (Glu^{203} in $G_{t\alpha}$; Glu^{207} in $G_{i\alpha1}$) could act as a general base. As in $G_{t\alpha}$, the carboxylate of Glu^{207} in $G_{i\alpha1}$ is turned away from the attacking water molecule (Fig. 6B); it forms a hydrogen bond with the main-chain carbonyl oxygen of residue 182 and an ion pair with Lys^{210}. (Lys or Arg is also conserved at this position in heterotrimeric G protein α subunits.) As suggested, a modest rotation would bring the Glu side chain into hydrogen bonding contact with the presumed water nucleophile but would require disruption of the two interactions observed in the native complexes. Furthermore, replacement of Glu^{207} by either Gln or Ala results in only slight (and equivalent) reductions in the k_{cat} for GTP hydrolysis (*38*). These data indicate that Glu^{207} does not play a substantial role in catalysis, at least in the absence of a GAP.

The picture that emerges from these studies is of a weak hydrolytic enzyme. Two residues, Arg^{178} and Gln^{204}, appear to play well-defined roles in a transition-state stabilization mechanism that we assume to be common to many G protein α subunits. The function of Gln^{61} in $p21^{ras}$ and its relatives may also be similar to that of the analogous Gln residue in G protein α subunits. There is no residue in either of these families of GTPases that is positioned to function as a general base to deprotonate the nucleophile. We presume that the absence of such a residue reflects a functional requirement for a hydrolytic site with weak activity. A slow GTPase permits maximal use of the free energy expended during the signal transduction process.

REFERENCES AND NOTES

1. A. G. Gilman, *Annu. Rev. Biochem.* **56**, 615 (1987).
2. H. R. Bourne, D. A. Sanders, F. McCormick, *Nature* **348**, 125 (1990); H. R. Bourne, D. A. Sanders, F. McCormick, *ibid.* **349**, 117 (1991); Y. Kaziro, H. Itoh, T. Kozasa, M. Nakafuku, T. Satoh, *Annu. Rev. Biochem.* **60**, 349 (1991); M. I. Simon, M. P. Strathmann, N. Gautam, *Science* **252**, 802 (1991).
3. J. R. Hepler and A. G. Gilman, *Trends Biochem. Sci.* **17**, 383 (1992).
4. D. T. Jones and R. R. Reed, *J. Biol. Chem.* **262**, 14241 (1987).
5. J. E. Buss, S. M. Mumby, P. J. Casey, A. G. Gilman, B. M. Sefton, *Proc. Natl. Acad. Sci. U.S.A.* **84**, 7493 (1987); M. E. Linder *et al.*, *ibid.* **90**, 3675 (1993).
6. M. E. Linder, D. A. Ewald, R. J. Miller, A. G. Gilman, *J. Biol. Chem.* **264**, 8243 (1990).
7. T. Higashijima, K. M. Ferguson, M. D. Smigel, A. G. Gilman, *ibid.* **262**, 757 (1987).
8. D. E. Logothetis, Y. Kurachi, J. Galper, E. J. Neer, D. E. Clapham, *Nature* **325**, 321 (1987); J. Iñiguez-Lluhi, C. Kleuss, A. G. Gilman, *Trends Cell Biol.* **3**, 230 (1993).
9. R. Taussig, W.-J. Tang, J. R. Hepler, A. G. Gilman, *J. Biol. Chem.* **269**, 6093 (1994).
10. F. McCormick, *Cell* **56**, 5 (1989); G. Berstein *et al.*, *ibid.* **70**, 411 (1992).
11. J. F. Eccleston and M. R. Webb, *J. Biol. Chem.* **257**, 5046 (1982); J. Feuerstein, R. S. Goody, M. R. Webb, *ibid.* **264**, 6188 (1989).
12. M. P. Graziano and A. G. Gilman, *ibid.*, p. 15475; M. Freissmuth and A. G. Gilman, *ibid.*, p. 21907.
13. M. Barbacid, *Annu. Rev. Biochem.* **56**, 779 (1987).
14. C. A. Landis *et al.*, *Nature* **340**, 692 (1989); J. Lyons *et al.*, *Science* **249**, 655 (1990).
15. E. F. Pai *et al.*, *Nature* **341**, 209 (1989).
16. M. Frech *et al.*, *Biochemistry* **33**, 3237 (1994).
17. G. G. Prive *et al.*, *Proc. Natl. Acad. Sci. U.S.A.* **89**, 3649 (1992).
18. J. P. Noel, H. E. Hamm, P. B. Sigler, *Nature* **366**, 654 (1993).
19. C. Van Dop, M. Tsubokawa, H. R. Bourne, J. Ramachandran, *J. Biol. Chem.* **259**, 696 (1984).
20. D. Cassel and Z. Selinger, *Proc. Natl. Acad. Sci. U.S.A.* **74**, 3307 (1977).
21. P. C. Sternweis and A. G. Gilman, *ibid.* **79**, 4888 (1982); J. Bigay, P. Deterre, C. Pfister, M. Chabre, *FEBS Lett.* **191**, 181 (1985); T. Higashijima, M. P. Graziano, H. Suga, M. Kainosho, A. G. Gilman, *J. Biol. Chem.* **266**, 3396 (1991).
22. W. A. Hendrickson, *Science* **254**, 51 (1991).
23. E. Lee, M. E. Linder, A. G. Gilman, *Methods Enzymol.* **237**, 146 (1994).
24. D. E. Coleman *et al.*, *J. Mol. Biol.* **238**, 630 (1994).
25. Crystals of native protein complexed with AlF_4^- were grown by the sitting drop method. Sitting drops containing 20 μl of protein (25 to 30 mg/ml), 300 μM $AlCl_3$, 5 mM NaF, 5 mM $MgCl_2$, 10 mM dithiothreitol (DTT), and 200 mM sodium acetate (pH 6.0) were equilibrated against 800 μl of 1.8 to 1.9 M ammonium sulfite at 21°C. Crystals grew in 14 to 21 days. To ensure that crystal forms were in similar environments during data collection, we transferred all crystals into a standard stabilization solution before data collection. This solution contained 100 mM *N,N*-bis[2-hydroxyethyl]-2-aminoethanesulfonic acid (BES) (pH 7.0), 1 mM $MgSO_4$, 1 mM GTPγS, 5 mM DTT, and either 88 percent saturated Li_2SO_4 for 7°C data sets or 75 percent saturated Li_2SO_4 and 15 percent glycerol for low-temperature data sets. Crystals of the GDP·AlF_4^-–$G_{i\alpha1}$ complex were stabilized as above except that 300 μM $AlCl_3$ and 5 mM NaF were substituted for GTPγS. The $K_3UO_3F_5$ and $UO_2(NO_3)_2$ derivatives were prepared by soaking crystals for 4 days in stabilization solution containing 1 mM heavy atom reagent and no DTT. All crystal forms belong to space group $P3_221$ with a and b = 80.5 Å, c = 106.5 Å. Crystals used for low-temperature data sets were flash-frozen in liquid nitrogen (*24*). Cell constants for frozen crystals are a,b = 79.5 Å, c = 105.5 Å. Selenomethionyl $G_{i\alpha1}$ was synthesized in the *E. coli* methionine auxotroph MIC 87 (provided by D. LeMaster, Northwestern University). Cells were transformed with the pQE-6–$G_{i\alpha1}$ and pREP4 plasmids and cultured in the presence of selenomethionine (*23*, *39*). Selenomethionyl $G_{i\alpha1}$ was purified with the same protocol as that used for native protein (*23*), except that the DEAE-Sephacel extraction and the Q-Sepharose chromatography steps were omitted and 10 mM DTT was used in all buffers. Yields of 7 to 15 mg per liter of culture were obtained. Electrospray quadrapole mass spectrometry of purified selenomethionyl $G_{i\alpha1}$ indicated 100 percent replacement of methionine with selenomethionine. The stoichiometry of GTPγS binding was similar to that for wild-type protein. Crystals of selenomethionyl GTPγS-$G_{i\alpha1}$ are isomorphous to wild-type crystals and are grown and prepared under the same conditions.
26. The structure of $G_{i\alpha1}$ was determined by molecular replacement. The coordinates of $G_{t\alpha}$ (*18*) from which GTPγS, Mg^{2+}, and the side chains of nonconserved residues had been removed were used as a search model. A clear solution for the rotation function was obtained by Patterson correlation refinement as implemented in X-PLOR [A. T. Brünger, *Acta Cryst.* **A46**, 46 (1990)], treating the helical and $p21^{ras}$-like domains as independent rigid bodies. (The magnitude of the true solution was 3.5 times that of the highest false peak.) The translation search provided a solution in the space group $P3_221$ which was consistent with the packing of the protein molecules in the unit cell. In the enantiomorphic space group $P3_121$, no such solution could be obtained. After rigid body refinement, inspection of a sigmaA-weighted $2F_o - F_c$ map [R. J. Read, *Acta Cryst.* **A42**, 140 (1986)] revealed obvious density for GTPγS and Mg^{2+}. At this stage, segments of polypeptide chain with poor density were deleted from the model before refinement was initiated in X-PLOR [A. T. Brünger, *X-PLOR Version 3.1. A System for X-ray Crystallography and NMR* (Yale Univ. Press, New Haven, 1992)]. During the course of refinement, missing parts of the protein structure and a number of bound solvent molecules were introduced into the model by means of the molecular graphics program O (*40*). Mutant GTPγS-$G_{i\alpha1}$ and native GDP·AlF_4^-–$G_{i\alpha1}$ structures were initially solved by difference Fourier techniques with the use of phases from the refined native GTPγS-$G_{i\alpha1}$ structure; these structures were then refined as above. In the

GDP·AlF_4^-·$G_{i\alpha1}$ structure, the geometry of the planar AlF_4^- complex and the new position of the hydrolytic water molecule were initially identified by $F_o - F_c$ maps from models containing protein and GDP only. A planar model for AlF_4^- consistent with known crystal structures was constructed and manually fit into the density. After unrestrained positional refinement, the model deviated only slightly from planar geometry with moderate shifts in bond lengths and angles. The model was again refined restraining the AlF_4^- in a square planar configuration with 1.78 Å Al-F bond distances (Table 2).
27. R. A. Laskowski, M. W. MacArthur, D. S. Moss, J. M. Thornton, *J. Appl. Crystallogr.* **26**, 283 (1993).
28. M. Antonelli, L. Birnbaumer, J. E. Allende, J. Olate, *FEBS Lett.* **340**, 249 (1994).
29. M. Mixon, D. E. Coleman, A. M. Berghuis, E. Lee, A. G. Gilman, S. R. Sprang, in preparation.
30. B. R. Conklin and H. R. Bourne, *Cell* **73**, 631 (1993).
31. D. G. Lambright, J. P. Noel, H. E. Hamm, P. B. Sigler, *Nature* **369**, 621 (1994).
32. A. M. de Vos *et al.*, *Science* **239**, 888 (1988); M. V. Milburn *et al.*, *Nature* **247**, 939 (1990).
33. The thermal parameter given is the average value for all side chain atoms in the residue. B_{ave} is the average B factor for all nonhydrogen atoms in the molecule. The B/B_{ave} normalization facilitates comparison of thermal parameters of equivalent atoms in different crystal complexes.
34. E. F. Pai *et al.*, *EMBO J.* **9**, 2351 (1990).
35. H. Berchtold *et al.*, *Nature* **365**, 126 (1993); M. Kjeldgaard, P. Nissen, S. Thirup, J. Nyborg, *Structure* **1**, 35 (1993).
36. The changes in the active site region of the GDP·AlF_4^- structure relative to the GTPγS-$G_{i\alpha1}$ form are unlikely to be caused by the different temperatures (100 and 300 K, respectively) at which the two data sets were collected. As a control, a selenomethionyl GTPγS-$G_{i\alpha1}$ data set collected at 108 K (λ = 0.9802 Å, Table 1) was used to generate $F_o - F_c$ and $2F_o - F_c$ maps after partial refinement with the native GTPγS-$G_{i\alpha1}$ model in which Arg^{178} and Gln^{204} were replaced with alanine. Electron density corresponding to the position of Arg^{178} and Gln^{204}, and the water nucleophile, as seen in the GTPγS-$G_{i\alpha1}$ structure, was observed in these maps. Thus, we conclude that cryocooling itself is not sufficient to affect the reorientation of these residues in the GDP·AlF_4^- complex.
37. Chung *et al.* [H.-H. Chung, D. R. Benson, P. G. Schultz, *Science* **259**, 806 (1993)] have shown that replacement of Gln^{61} with a nitroglutamine analog in $p21^{ras}$ yields an enzyme that has full catalytic activity and retains the ability to be stimulated by GAP. Nitroglutamine is isosteric and isoelectronic with glutamine, but cannot serve as a hydrogen bond donor. Further, it is a weak hydrogen bond acceptor. It may be that nitroglutamate distorts GTP toward the transition state or stabilizes an active conformation state of the protein. It is also possible that the dipole moment of the nitro moiety may be exploited to orient the water molecule for nucleophilic attack and to stabilize developing charge in the transition state. The full activity of the nitro mutant suggests that such mechanisms are sufficient to explain the role of Gln^{61} in the wild-type enzyme as well. However, $p21^{ras}$ is a relatively weak enzyme, and much of its activity might be attributed to entropic stabilization of the reactive species in the active site. Additional degrees of rate enhancement could be achieved by several different (or combinations of) mechanisms might include the basicity and the dipolar or hydrogen bonding properties of a residue that happens to be positioned at the site occupied at Gln^{61}. Thus, we cannot ignore the obvious potential role of hydrogen bonding in transition state stabilization by Gln^{204} in $G_{i\alpha1}$.
38. C. Kleuss, A. S. Raw, E. Lee, S. R. Sprang, A. G. Gilman, *Proc. Natl. Acad. Sci. U.S.A.*, in press.
39. S. Doublie, Jr. and C. W. Carter, in *Crystallization of Nucleic Acids and Proteins: A Practical Approach*, A. Ducruix and E. Giege, Eds. (Oxford Univ. Press, New York, 1992), p. 311.
40. T. A. Jones, M. Bergdoll, M. Kjeldgaard, in *Crystallographic and Modeling Methods in Molecular Design*, C. E. Bugg and S. E. Ealick, Eds. (Springer-Verlag, New York, 1990), p. 189.
41. A. T. Brünger, *Nature* **355**, 472 (1992).
42. P. J. Kraulis, *J. Appl. Crystallogr.* **24**, 946 (1991).
43. D. J. Bacon and W. F. Anderson, *J. Mol. Graphics* **6**, 219 (1988).
44. J. K. Northup, M. D. Smigel, A. G. Gilman, *J. Biol. Chem.* **257**, 11416 (1982).
45. E. Lee, R. Taussig, A. G. Gilman, *ibid.* **267**, 1212 (1992).
46. Z. Otwinowski, in *Data Collection and Processing*, L. Sawyer, N. Isaacs, S. Bailey, Eds. (Science and Engineering Research Council, Warrington, United Kingdom, 1993), pp. 56–62.
47. J. L. Smith, E. J. Zalvzec, J.-P. Wery, Y. Satow, in *Isomorphous Replacement and Anomalous Scattering*, W. Wolf, P. R. Evans, A. G. W. Leslie, Eds. (Science and Engineering Research Council, Warrington, United Kingdom, 1991), pp. 96–106.
48. Z. Otwinowski, in *Isomorphous Replacement and Anomalous Scattering*, W. Wolf, P. R. Evans, A. G. W. Leslie, Eds. (Science and Engineering Research Council, Warrington, United Kingdom, 1991), pp. 80–86.
49. *CCP4, The SERC (UK) Collaborative Computing Project No. 4: A Suite of Programs for Protein Crystallography* (Warrington, United Kingdom, Daresbury Laboratory, 1991).
50. We thank J. Noel and P. Sigler for coordinates of GTPγS-$G_{i\alpha}$; W. Hendrickson and C. Ogata for assistance with the use of the Howard Hughes Medical Institute beamline (X4a) at the National Synchrotron Light Source and for valuable discussions with regard to MAD phasing; M. Graziano for the first supplies of G_α protein for crystallization; C. Nguyen for assistance with mutant protein synthesis; C. Slaughter for assistance with mass spectrometry; Z. Wang, B. Sutton, M. Mixon, and J. Naismith for help with data collection; and P. Sternweis and C. Jones for technical assistance. Supported by NIH grant DK 46371 (S.R.S.) and Welch Foundation grant I-1229 (S.R.S.); NIH grant GM34497, American Cancer Society grant BE30-O, and Welch Foundation grant I-1271 (A.G.G.); and the Lucille P. Markey Charitable Trust and the Raymond Willie Chair of Molecular Neuropharmacology. Coordinates have been deposited with the protein data bank, accession code number 1GIA.

18 July 1994; accepted 8 August 1994